Deformation behavior of non-rigid airships in wind tunnel tests

Article *in* Chinese Journal of Aeronautics · March 2019

DOI: 10.1016/j.cja.2018.12.016

4 authors:


Lingling Lu
Chinese Academy of Sciences


Hong-Wei Song
Chinese Academy of Sciences


Yiwei Wang
Chinese Academy of Sciences


Chenguang Huang
Chinese Academy of Sciences

Chinese Journal of Aeronautics, (2019), xxx(xx): xxx–xxx

Chinese Society of Aeronautics and Astronautics
& Beihang University

Chinese Journal of Aeronautics

cja@buaa.edu.cn
www.sciencedirect.com

Deformation behavior of non-rigid airships in wind tunnel tests

Lingling LU [a], Hongwei SONG [a,b], Yiwei WANG [a,b,*], Chenguang HUANG [a,b]

[a] *Key Laboratory for Mechanics in Fluid Solid Coupling Systems, Institute of Mechanics, Chinese Academy of Sciences, Beijing 100190, China*
[b] *School of Engineering Science, University of Chinese Academy of Sciences, Beijing 100049, China*

Received 21 January 2018; revised 12 December 2018; accepted 12 December 2018

KEYWORDS

Angle of.attack;
Fiber Bragg grating sensor;
Flow velocity;
Internal pressure;
Non-rigid airship;
Wind tunnel test

Abstract Deformation behavior of non-rigid airships in wind tunnel tests is studied by considering three factors, including internal pressure, flow velocity and angle of.attack. Fiber Bragg grating strain sensors are used to measure the deformation of non-rigid airships. Wind tunnel tests in the case of different flow velocities and attack angles are conducted. The measurement results reveal that the airship deformation is in proportion to internal pressure. For the tensile region, the airship deformation is in proportion to flow velocity. Effects of angle of.attack on structural deformation are more complicated and there is no clear relationship existing between airship deformation and angle of.attack.

1. Introduction

Airships, as a class of lighter-than-air aircraft, are important platforms for transportation and observation in the air. On the basis of their hull structure configuration, airships can be classified into three categories, namely, rigid, non-rigid, and semi-rigid airships.[1] They are the first aircraft that realized mankind's ambition of a controlled, powered flight.[2] Airships have a significant range of performance capabilities that can be exploited. One main advantage of airships is the low-cost energy consumption. Airships can hover for a long time without refueling and with low operating costs. Additionally, they can be boarded without long runway, enabling them to transport heavy cargoes in remote areas. Airships can meet the challenging tasks in which airplanes and helicopters are not well-suited. Therefore, a wide range of applications have been recently proposed for modern airships in commercial, scientific, and military fields, such as advertising and tourism[3], environmental monitoring[4,5], planetary exploration[6,7], heavy lift cargo transport[8] and stratospheric observation and telecommunication relay.[9,10]

Non-rigid airships with inflated envelopes are the most common type of airships. Given that airships can be easily deformed, two aspects of fluid-structure coupling issues should be considered, which are the deformation of airships in flight

* Corresponding author at: Key Laboratory for Mechanics in Fluid Solid Coupling Systems, Institute of Mechanics, Chinese Academy of Sciences, Beijing 100190, China.
E-mail address: wangyw@imech.ac.cn (Y. WANG).

Peer review under responsibility of Editorial Committee of CJA.

Production and hosting by Elsevier

https://doi.org/10.1016/j.cja.2018.12.016
1000-9361

and the influences of this deformation on the aerodynamic characteristics of airships.[11] Numerical simulation is the main approach for analyzing the effects of the fluid-structure interaction of airships.[12–15] However, experimental study on airship fluid-structure interaction is scarce, and no quantitative result on the structural deformation of airships is found (from wind tunnel or flight tests). Many difficulties exist for the experimental measurement of deformation behavior of non-rigid airships. On the one hand, the traditional strain gauge significantly increases the weight of non-rigid airships in flight testing and requires many additional equipment and wires. In this case, the vibration and deformation properties of airships would change significantly, obtaining unreal experimental data. On the other hand, non-contact methods, such as digital image correlation,[16–18] as an optical measurement method, are unsuitable for measuring the deformation of airships in wind tunnel and flight tests. Since the cameras should be placed outside the wind tunnel, the credibility and accuracy of measurement decrease. Therefore, effective measurement methods should be developed to obtain the deformation behavior of non-rigid airships.

In the present study, wind tunnel tests on non-rigid airship and deformation measurements are performed. A typical non-rigid airship model and Fiber Bragg Grating (FBG) strain sensors are used to measure structural response. Effects of internal pressure, flow velocity, and angle of.attack on the deformation behavior of non-rigid airships are analyzed. The paper is organized as follows: the rationality of the proposed measuring method is discussed in Section 2. In Section 3, the experimental setup of wind tunnel tests is introduced. In Section 4, the influences of internal pressure, flow velocity, and angle of.attack on the deformation of non-rigid airships are discussed and analyzed. Several conclusions are presented in Section 5.

2. Validation of measurement technique

To measure airship deformation, FBG sensor is selected. On the one hand, an FBG sensor is lightweight with a minimal influence on the intrinsic vibration and deformation behavior of non-rigid airships. On the other hand, an FBG sensor has small physical dimensions, which is suitable to be embedded or attached to a structure. Moreover, no additional wire is required to connect the sensors to the control system because the fibers themselves act as the sensing elements and the signal propagation conduits.[19,20] Therefore, FBG sensor is suitable to measure the deformation of non-rigid airships in wind tunnel and flight tests.

In the following subsection, tensile tests of thin membranes with fixed FBG sensors were conducted to verify that the measuring method is suitable for the measurement of non-rigid airships.

2.1. Tensile tests of thin films

In the tests, the material of the thin film is the same with the film that is constructed in non-rigid airship, and dimensions of the specimen are: the tensile length $L = 4$ cm, width $w = 7$ mm, and thickness $d = 0.08$ mm. The thin membranes are shown in Fig. 1(a), and the distance between the two red lines is the tensile length.

FBG strain sensor was fixed on the thin film by using acrylic resin, as shown in Fig. 1(b). Instron 5848 micro-tester was used to conduct the tensile tests with a loading rate of 0.2 mm/min at room temperature. SM125 equipment was used to sample and demodulate the signal of the FBG strain sensor with a sample frequency of 2 Hz. Three tensile tests on the thin membrane were conducted to evaluate the reliability of the measuring method.

2.2. Test results

Stress σ and engineering strain ε can be obtained by

$$\sigma = F/(wd) \tag{1}$$

$$\varepsilon = \Delta L/L \tag{2}$$

where F is the loading force, and w and d are the width and thickness of the thin membrane specimen respectively, ε is the engineering strain, ΔL is the tensile displacement, and L is the tensile length.

The obtained stress-strain curves are shown in Fig. 2. From Fig. 2, the elastic modulus of the three tests is the same, which demonstrates that the tensile tests are reliable. The measurement result of the FBG sensor is not the real strain of the tested thin membrane, because the stiffness of the FBG sensor is much higher than the thin membrane and the glue also influenced the stiffness of the thin membrane. However, it is seen that the measurement results of FBG sensors in Fig. 3 can reflect the deformation law of thin film by multiplying a modified coefficient. The strain value of the FBG sensor is very close to the estimated engineering strain by multiplying a mod-

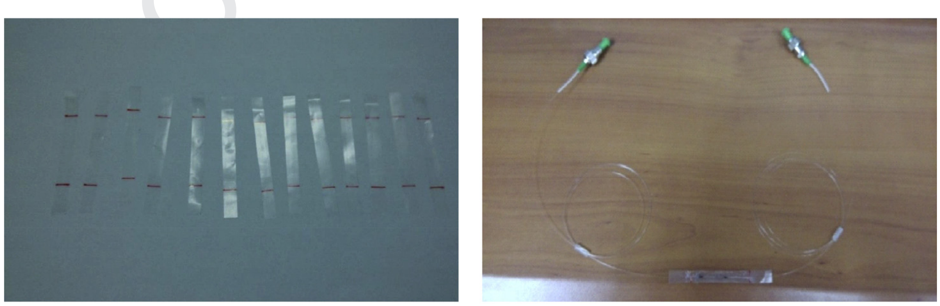

(a) Thin membrane specimen (b) Thin membrane with fixed FBG sensor

Fig. 1 Specimens of thin membranes.

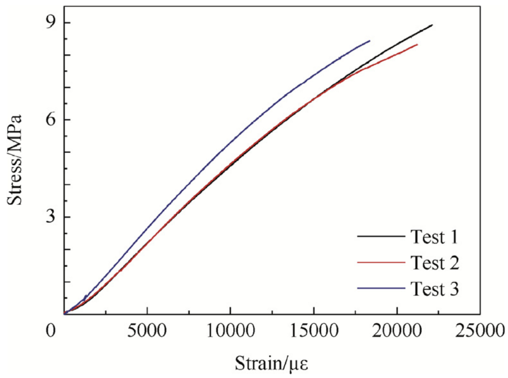

Fig. 2 Stress-strain curves obtained from tests.

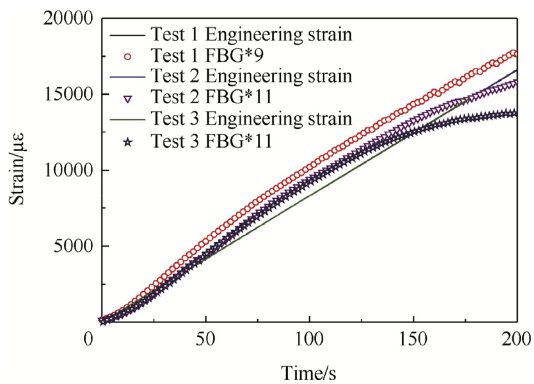

Fig. 3 Strain history of tensile tests.

ified coefficient. The modified coefficients for the three tests are 9, 11 and 11 respectively. Although the modified coefficients vary in different tests, they are always around a constant number. Therefore, FBG sensors can be used to measure the deformation behavior of non-rigid airships.

3. Test procedure

3.1. Wind-tunnel tests setup

Wind tunnel tests with a non-rigid airship are conducted in the low-speed wind tunnel at the China Academy of Aerospace Aerodynamics. The layout of experimental system and distribution of FBG sensors are shown in Fig. 4. The cross section of the wind tunnel is 3 m × 3 m. The non-rigid airship model is composed of 12 pieces of PolyVinyl Chloride (PVC) thin film. The length of the airship model is about 2.3 m. The maximum diameter of the non-rigid airship model is 0.6 m. The arrangement of the rudders follows the Y type. The whole airship is supported by a rigid support bar, which can change automatically with the expansion of the envelope. The inflow velocity is 10 and 15 m/s, and the angle of.attack of the airship varies from 0° to 20° and 0° to 12°, respectively.

Fig. 4(b) shows the zoomed airship attached with FGB sensors. The sensor layout and numbering are shown in Fig. 4(c). Six pieces of membrane are selected for the placement of the FBG sensors, because the non-rigid airship is a symmetrical structure. A total of 18 FBG sensors are placed in longitudinal direction, and another 18 FBG sensors are placed in circumferential direction. The sample frequency of FBG sensors is 50 Hz.

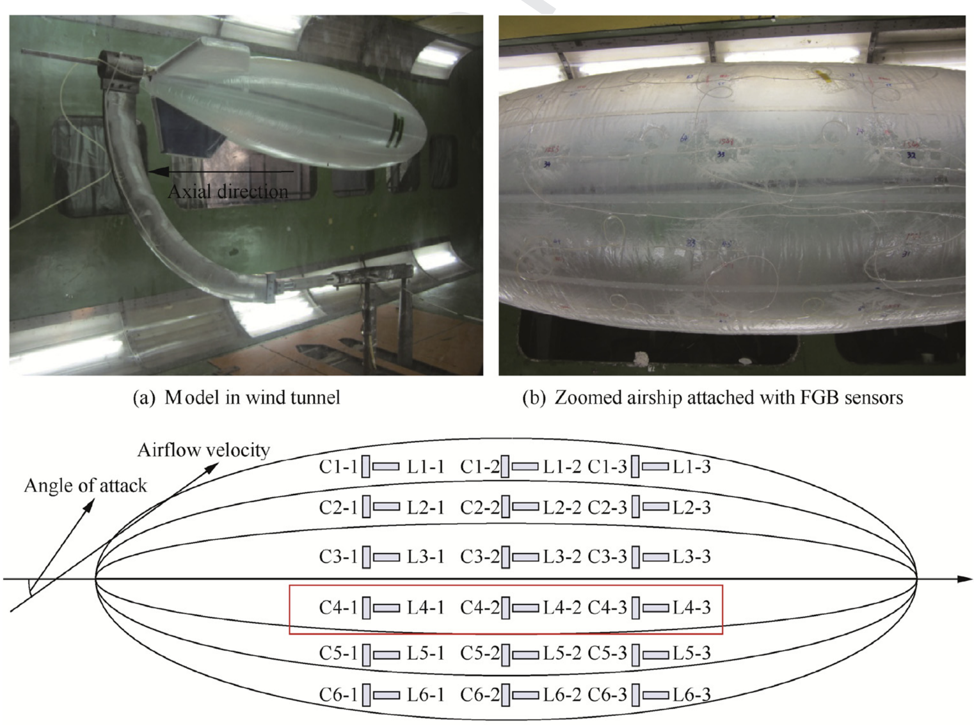

(a) Model in wind tunnel (b) Zoomed airship attached with FGB sensors

Note: "L" and "C" represent longitudinal and circumferential directions, respectively.

(c) Layout and numbering of sensors

Fig. 4 Experimental setup of wind tunnel test.

Please cite this article in press as: LU L et al. Deformation behavior of non-rigid airships in wind tunnel tests, *Chin J Aeronaut* (2019), https://doi.org/10.1016/j.cja.2018.12.016

Table 1 Information of four groups of tests.

Test No.	v (m/s)	$P_{initial}$ (Pa)	θ (°)
Test 1	10	1200	0–20
Test 2	10	1200	20–0
Test 3	15	1200	0–12
Test 4	15	1200	12–0

3.2. Test information

In the tests, the influences of three factors, including internal pressure P, angle of.attack θ, and flow velocity v, on airship deformation are considered. Four tests are conducted as shown in Table 1. The flow velocities include 10 and 15 m/s. In the test, angle of.attack θ of airship varies at every 2°. The initial internal pressure $P_{initial}$ is set as 1200 Pa. As θ changes, the internal pressure of the airship decreases, because the airship cannot be sealed completely and no air is blown into the airship after the test begins. In each test, the initial and final internal pressures ($P_{initial}$ and P_{final}) corresponding to different θ are recorded.

4. Test results and discussion

4.1. Overall test results

In this section, effects of internal pressure, flow velocity, and angle of.attack on structural deformation are discussed. On the same film, six sensors, including Sensors L4-1, L4-2, L4-3, C4-1, C4-2 and C4-3 are selected (see Fig. 4(c)).

In each test, strain results with the same θ are averaged over measured period, and the results are shown in Fig. 5. From Fig. 5, tendencies of three axial sensors are similar, and the same conclusion can also be found for three radial sensors. These results demonstrate that the measuring method accurately reflects the deformation law, although it could not obtain actual deformation values.

Referring to Table 1, internal pressure P drops as angle of. attack θ increases in Test 1 and Test 3, whereas P drops as θ decreases in Test 2 and Test 4. From Fig. 5(b), as angle of.attack θ increases and internal pressure P decreases (Tests 1 and 3), the circumferential strain diminishes. In Fig. 5(a), longitudinal strain decreases at the beginning, and then increases. In Tests 2 and 4, the longitudinal and circumferential strains decrease as θ and P are reduced. These results demonstrate that the effect of internal pressure on circumferential deformation is greater than that on longitudinal deformation. The

Table 2 Information of four selected cases.

Case No.	v (m/s)	θ (°)	$P_{initial}$ (Pa)	P_{final} (Pa)
Test 1_2	10	2	1184	1176
Test 2_2	10	2	1030	1025
Test 3_4	15	4	1163	1156
Test 4_4	15	4	1106	1097

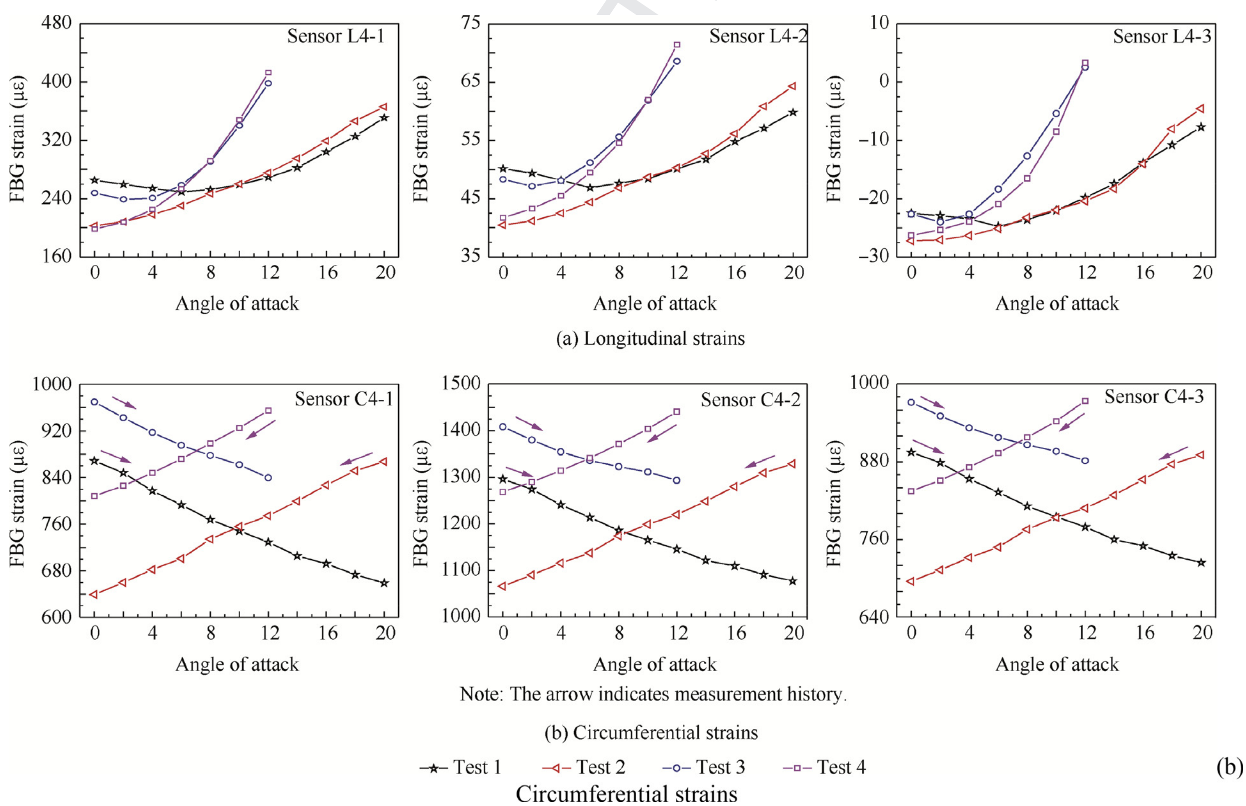

Fig. 5 Responses of average strains.

Please cite this article in press as: LU L et al. Deformation behavior of non-rigid airships in wind tunnel tests, *Chin J Aeronaut* (2019), https://doi.org/10.1016/j.cja.2018.12.016

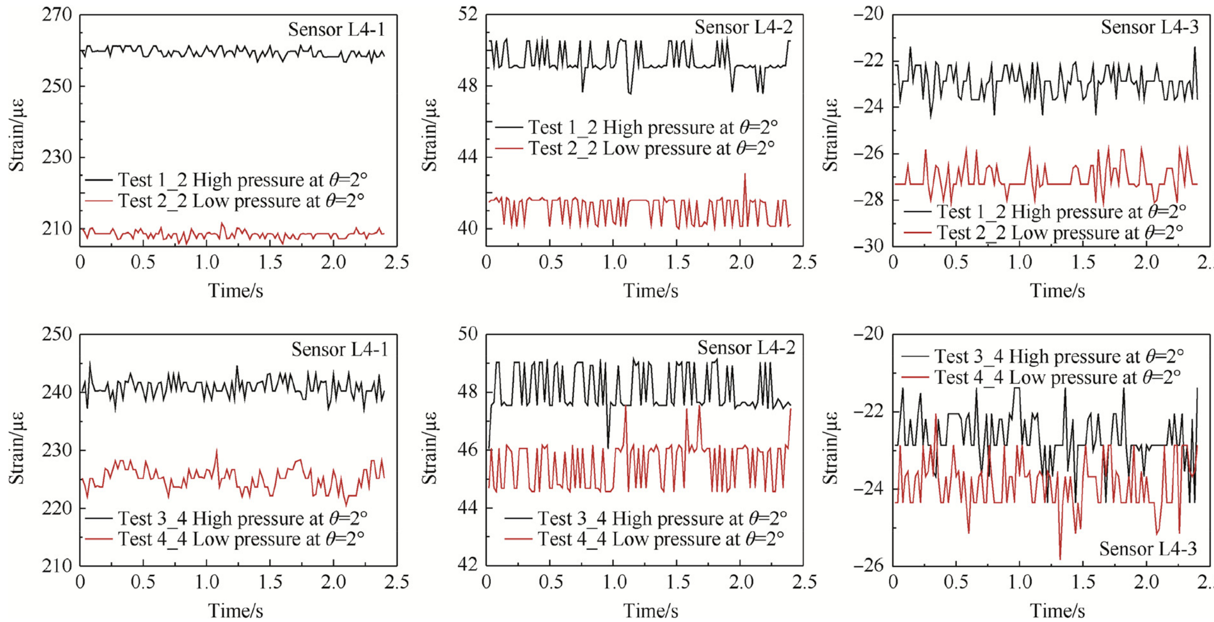

Fig. 6 Influence of internal pressure on longitudinal strain.

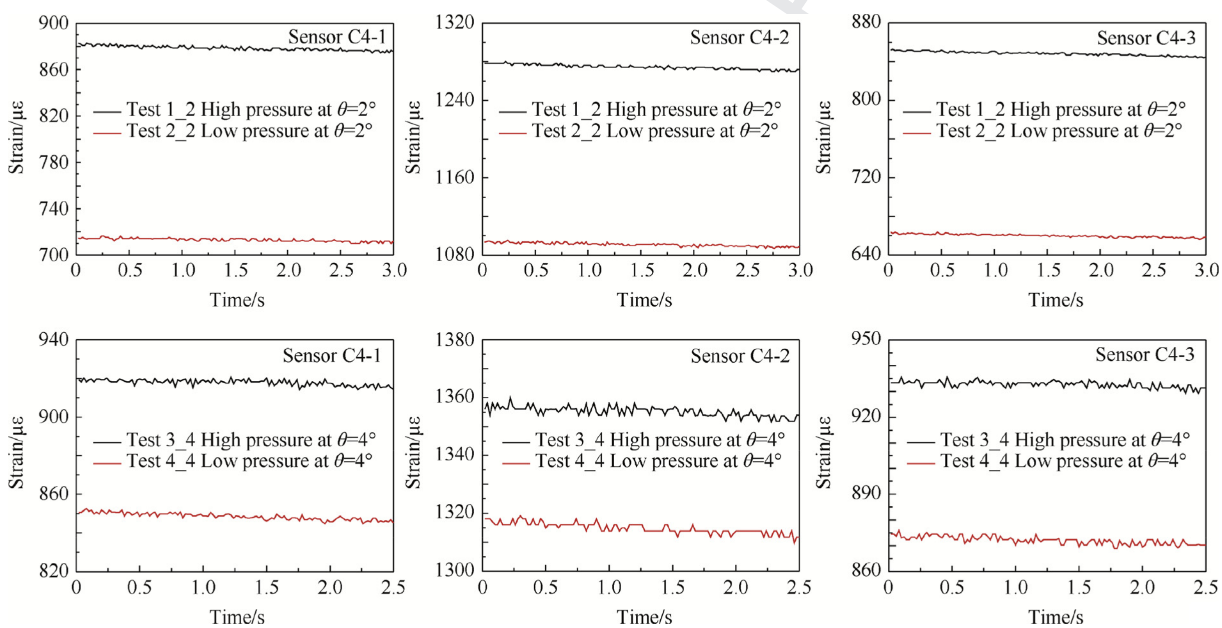

Fig.7 Influence of internal pressure on circumferential strain.

effect of angle of.attack on structural longitudinal deformation is greater than that of internal pressure.

In the wind tunnel test, values of all FBG sensors are offset to zero after a certain amount of air blown into airship and before wind tunnel is started. After the wind tunnel is started, values of FBG sensors in the compressed zones become negative, such as Sensor L4-3. When the stretching force is applied, the state of the FBG sensor will change from compressive to tensile, and the strain value of Sensor L4-3 will change from a negative to a positive value.

4.2. *Effects of internal pressure*

Cases with the same flow velocity v and angle of.attack θ are selected to analyze the effects of internal pressure on non-rigid airship deformation. Test 1_2 and Test 2_2, Test 3_4 and Test 4_4 are selected and detail information is supplied in Table 2.

According to Fig. 6, it is seen that the longitudinal strain of Test 1_2 and Test 3_4 is larger than the corresponding longitu-

Table 3 Information of six selected cases.

Case No	v (m/s)	θ (°)	P_{initial} (Pa)	P_{final} (Pa)
Test 1_0	10	0	1200	1197
Test 3_0	15	0	1200	1194
Test 1_2	10	2	1184	1176
Test 3_2	15	2	1182	1174
Test 1_4	10	4	1163	1156
Test 3_4	15	4	1163	1156
Test 1_6	10	6°	1146	1140
Test 3_6	15	6	1146	1141

dinal strain of Test 2_2 and Test 4_4. And the same conclusion could also been obtained according to circumferential strain results in Fig. 7. From Figs. 6 and 7, it is also seen that measured strains decrease gradually with time, due to internal pressure drop once inflated. For the non-rigid airship, as the internal pressure increases, volume of non-rigid airship increases. Therefore, the local deformation of a non-rigid airship increases, and the local longitudinal and circumferential strains increase. Test results are in accordance with the analytical results. Moreover, test results and analytical results also verify the reliability of the non-rigid airship measurement method based on FBG sensor.

4.3. Effects of flow velocity

Influences of flow velocity on non-rigid airship deformation are analyzed. Test 1_0 to Test 1_6 and Test 3_0 to Test 3_6 are selected, and the information of the selected tests are shown in Table 3. The average strain values of six sensors with the full time response are provided in Fig. 8.

In Fig. 8, when angle of.attack θ is small, longitudinal strains in the case of velocity 10 m/s are larger than those in the case of velocity 15 m/s. As θ increases, longitudinal strains in the case of 10 m/s drop, whereas longitudinal strains rise in the case of 15 m/s. When θ is larger than 0° and the wind load is applied, the airship model subjects to a bending moment. As θ increases, the bending moment of airship model increases, and longitudinal strains of sensors placed in the tensile region would increase, whereas longitudinal strains of sensors placed in the compression region decrease. When θ is small, the internal pressure is the main factor that accounts for variation of strains. And the flow velocity becomes the dominant influence factor as θ increases. That is the reason for the tendency given in Fig. 8(a). From Fig. 8(b), it is seen that the circumferential strain increases as the flow velocity increases from 10 m/s to 15 m/s. For sensors on the tensile region, the circumferential strain is in proportion to the flow velocity.

According to Fig. 8(a) and (b), measured strains decrease as the angle of.attack increases, expect longitudinal stains of Test 3. Because the internal pressure decreases as θ increases, then strain value decreases. However, when θ is large, the effect of flow velocity on airship deformation is larger than that of internal pressure. Therefore longitudinal stains of Test 3 decrease at first and then increase.

4.4. Effects of angle of.attack

Four cases with the same internal pressure and flow velocity are selected to investigate the influence of angle of.attack on airship deformation and detailed information is shown in Table 4. The measurement results are applied in Fig. 9.

In Fig. 9, strains of several measured locations are proportional to θ. However, some measured locations are inversely proportional to θ. No clear relationship exists between defor-

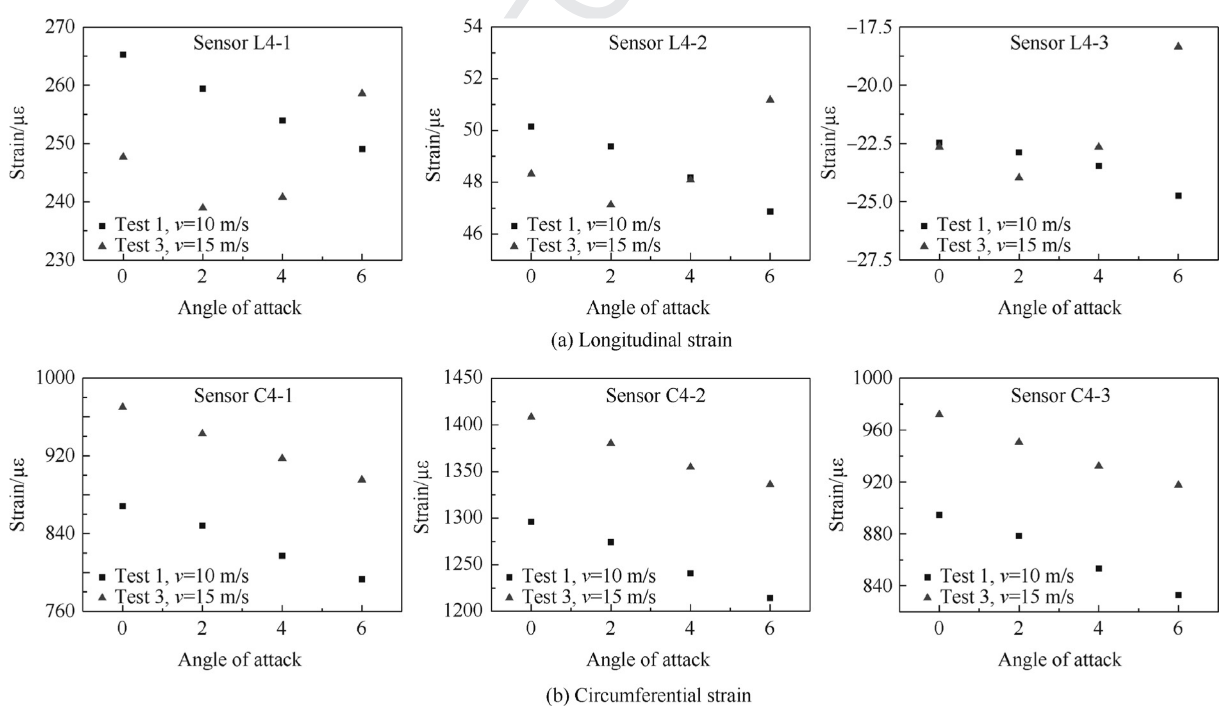

Fig. 8 Influence of airflow velocity on longitudinal strain and circumferential strain.

Please cite this article in press as: LU L et al. Deformation behavior of non-rigid airships in wind tunnel tests, *Chin J Aeronaut* (2019), https://doi.org/10.1016/j.cja.2018.12.016

Table 4 Information of four selected cases.

Case No.	v (m/s)	θ (°)	P_{initial} (Pa)	P_{final} (Pa)
Test 1_8	10	8	1127	1120
Test 2_12	10	12	1127	1118
Test 3_0	15	0	1200	1194
Test 4_12	15	12	1200	1194

mation and angle of.attack θ, as the influence of θ on structural deformation is determined by the bending moment applied to the non-rigid airship. The bending moment of the model is affected by many factors, including the rod stiffness, the internal pressure of airship and flow velocity. Therefore, effects of θ on structural deformation are more complicated than those of internal pressure and flow velocity.

5. Conclusions

In this study, wind tunnel tests for non-rigid airships are conducted, and the influences of internal pressure, flow velocity, and angle of.attack on airship deformation are analyzed. In the work, FBG sensors are used to measure airship deforma-

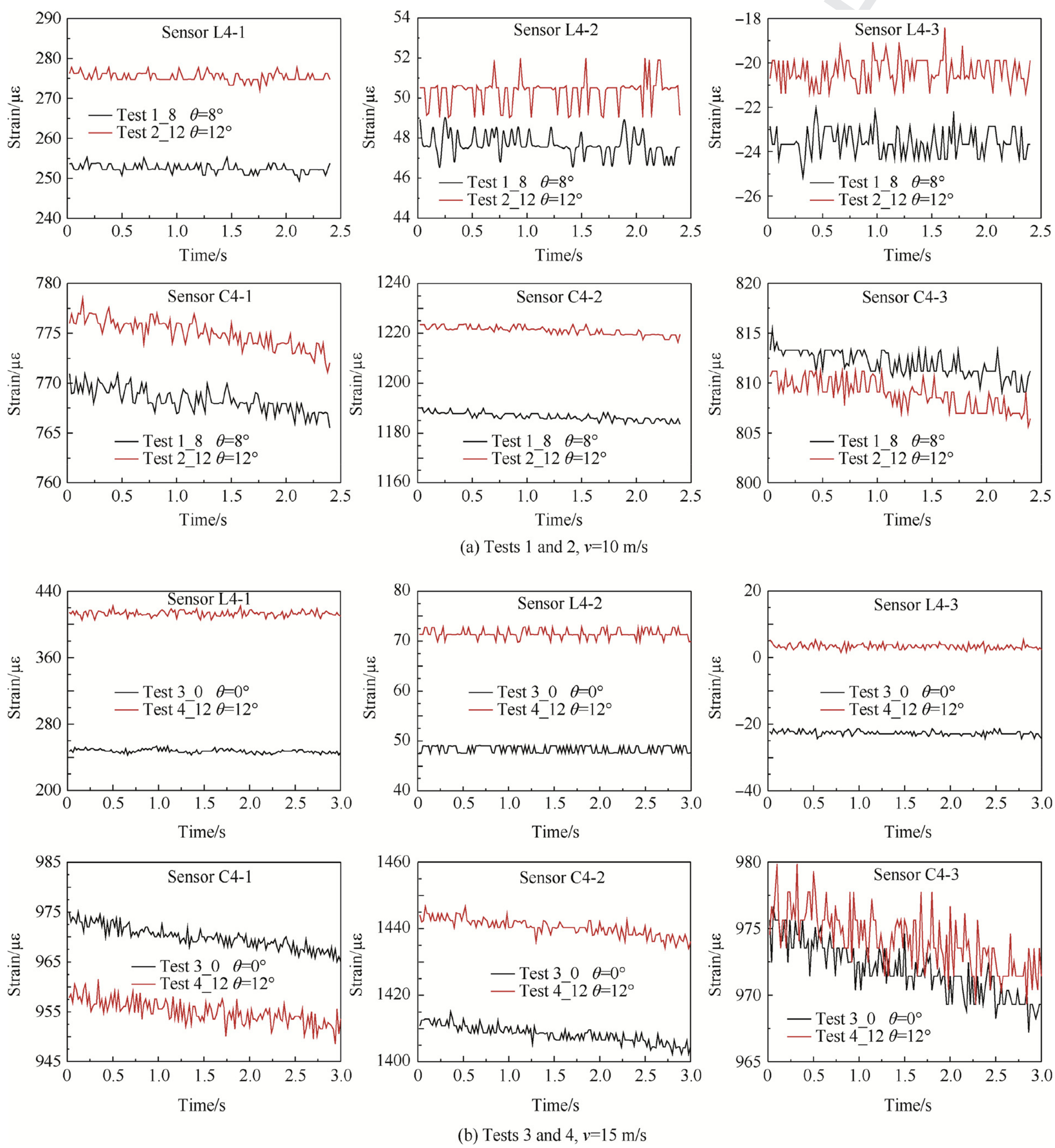

(a) Tests 1 and 2, v=10 m/s

(b) Tests 3 and 4, v=15 m/s

Fig. 9 Influence of angle of.attack.

tion. FBG sensor and the corresponding pasted PVC film are considered as a whole, which is used to measure the deformation behavior of the whole airship. Based on the test results, some conclusions are obtained:

(1) The deformation of the non-rigid airship is in proportion to the internal pressure.
(2) For the tensile region of airship, the longitudinal and circumferential strains are in proportion to the flow velocity.
(3) Effects of angle of.attack on airship deformation are complicated and should be analyzed with the internal pressure and flow velocity. Bending moment is the main source for the variation of strains. More works need to be conducted to investigate the relationship between structural deformation and angle of.attack.

Acknowledgement

This research is supported by the National Natural Science Foundation of China (Nos. 11472276, 11332011 and 11502268).

Appendix A. Supplementary data

Supplementary data to this article can be found online at https://doi.org/10.1016/j.cja.2018.12.016.

References

1. Liao L, Pasternak I. A review of airship structural research and development. *Prog Aerosp Sci* 2009;**45**:83–96.
2. Li YW, Nahon M, Sharf I. Airship dynamics modeling: a literature review. *Prog Aerosp Sci* 2011;**47**:217–39.
3. Oh S, Kang S, Lee K, Ahn S, Kim E. Flying display: Autonomous blimp with real-time visual tracking and image projection 2006 Oct 9-15*Proceedings of the IEEE/RSJ international conference on intelligent robots and systems*. Beijing, China: Piscataway: IEEE Press; 2006. p. 131–6.
4. Dorrington GE. Development of an airship for tropical rain forest canopy exploration. *Aeronaut J* 2005;**109**:361–72.
5. Kulczycki EA, Joshi SS, Hess RA, Elfes A. Towards controller design for autonomous airship using SLC and LQR methods 2006 Aug 21–24*AIAA Guidance, navigation and control conference and exhibit*. Keystone, USA: Reston: AIAA; 2006. p. 21–4.
6. Elfes A, Bueno SS, Bergerman M, Paiva ECD, Ramos JG, Azinheira JR. Robotic airships for exploration of planetary bodies with an atmosphere: autonomy challenges. *Auton Robot* 2003;**14**(2–3):147–64.
7. Kusagaya T, Kojima H, Fujii HA. Estimation of flyable regions for planetary airships. *J Aircraft* 2006;**43**(4):1177–81.
8. Pope C. The big lift. *Prof Eng* 2004;**17**(8):24–5.
9. Schmidt DK. Modeling and near-space station keeping control of a large high- altitude airship. *J Guid Control Dynam* 2007;**30**(2):540–7.
10. Lee S, Bang H. Three-dimensional ascent trajectory optimization for stratospheric airship platforms in the jet stream. *J Guid Control Dynam* 2007;**30**(5):1341–52.
11. Wu XC, Wang YW, Huang CG, Liu YB, Lu LL. Experiment and numerical simulation on the characteristics of fluid-structure interactions of non-rigid airships. *Theor Appl Mech Lett* 2005;**5**:258–61.
12. Liu J, Lu C, Xue L. Investigation of airship aeroelasticity using fluid-structure interaction. *J Hydrodyn Ser B* 2008;**20**:164–71.
13. Liu JM, Lu CJ, Xue LP. Numerical investigation on the aeroelastic behavior of an airship with hull-fin configuration. *J Hydrodyn Ser B* 2010;**22**:207–13.
14. Wang C, Du X, Wan Z. An experimental study on wrinkling behaviours and characteristics of gossamer space structures. *Strain* 2007;**43**:332–9.
15. Kang WG, Suh YW, Woo K. Mechanical property characterization of film-fabric laminate for stratospheric airship envelope. *Compos Struct* 2006;**75**:151–5.
16. Yamaguchi I. Simplified laser-speckle strain gauge. *Opt Eng* 1982;**21**:436–40.
17. Peters WH, Ranson WF. Digital imaging techniques in experimental stress analysis. *Opt Eng* 1982;**21**:427–31.
18. Niendorf T, Dadda J, Canadinc D, Maier HJ, Karaman I. Monitoring the fatigue-induced damage evolution in ultrafine-grained interstitial-free steel utilizing digital image correlation. *Mat Sci Eng A Struct* 2009;**517**:225–34.
19. Berkoff TA, Kersey AD. Fiber Bragg grating array sensor system using a bandpass wavelength division multiplexer and interferometric detection. *IEEE Photonic Tech L* 1996;**8**(11):1522–4.
20. Majumder M, Gangopadhyay TK, Chakraborty AK, Dasgupta DK, Bhattacharya DK. Fibre Bragg gratings in structural health monitoring—Present status and applications. *Sens Actuat A-Phys* 2008;**147**:150–64.